JOURNAL OF GEOPHYSICAL RESEARCH, VOL. 92, NO. D4, PAGES 4287–4296, APRIL 20, 1987

Reflectivity of Earth's Surface and Clouds in Ultraviolet From Satellite Observations

T. F. ECK,[1] P. K. BHARTIA,[2] P. H. HWANG,[3] AND L. L. STOWE[4]

The Total Ozone Mapping Spectrometer (TOMS) on board Nimbus 7 is used to infer the ultraviolet (UV) surface and cloud reflectance at 370 nm. Cloudless surface reflectivity was analyzed on a global basis for all surface types for several months. The UV surface reflectivity varies from 2% for some forest and grassland regions to 14% for some sandy desert areas. A notable exception is the large salt flats of Bolivia, which have a reflectivity of ~60%. Cloud reflectivity was also analyzed for clouds located at three levels in the atmosphere, as determined by the 11.5-μm channel of the Temperature Humidity Infrared Radiometer. Average cloud reflectivity at 370 nm ranges from 52% for low clouds (tops <2 km) to 76% for high clouds (tops >7 km at the equator, decreasing to >4 km at poles).

1. INTRODUCTION

Information on the reflection of incident solar energy from natural surfaces is important for radiative transfer studies within the atmosphere. For the ultraviolet (UV) wavelengths, knowledge of reflectivity is of concern in photochemical studies of both the troposphere and lower stratosphere. Reflected UV radiation is also of interest in studies to ascertain the biological and physiological effects of UV radiation on plants and animals and for problems of remote sensing which require characterizing the signatures of various planetary features, such as environmental and earth-resources monitoring from satellites.

Although there is an abundance of literature on albedo and reflectivity in the visible region, there is still very little information on the UV reflectivity of natural surfaces. *Doda and Green* [1980] measured the UV reflectance of four different kinds of surfaces from an airplane under cloudless conditions. *Frederick and Abrams* [1981] provided statistics on the earth and cloud albedo in the tropics for the 340- to 350-nm band from the backscattered ultraviolet (BUV) instrument on the Atmospheric Explorer E satellite. *Ashburn and Weldon* [1956] measured the visible spectral reflectance of several desert surfaces, including measurements made at 400 nm from the ground and from a low-altitude helicopter. *Hulburt* [1928] made laboratory measurements of the UV reflectance of snow, sand, and other substances for the 300- to 400-nm band. Even if many more surface observations of UV reflectivity were available, these observations may not meet the needs of studies requiring global coverage. This paper is concerned with evaluating the UV reflectance data obtained from the Total Ozone Mapping Spectrometer (TOMS) instrument on the Nimbus 7 satellite and is a global study of UV reflectance of the earth's surface features and clouds.

2. EXPERIMENTAL TECHNIQUE

The TOMS instrument on board the Nimbus 7 satellite measures the backscattered radiance from the earth in six 1-nm-wide spectral bands in the UV, centered at 380, 360, 340, 331, 318, and 313 nm. It also measures the incoming solar flux at these bands, which are used to convert the radiances into directional albedos.

Field of view of the TOMS instrument is 50 × 50 km in the nadir direction, increasing to 150 × 200 km in the extreme off-nadir direction. Local noon orbit and a cross-track scanning feature allows a complete daily coverage of the globe except for those areas of the polar region that are in darkness throughout the day.

In the TOMS reflectivity algorithm described here, one obtains a "scene reflectivity" from the albedos measured at the two longest wavelength bands centered at 380 and 360 nm. After *Dave* [1964], the directional albedo A of a Rayleigh-scattering atmosphere of optical depth τ bounded by an opaque lambertian surface of reflectivity R is given by

$$A = \frac{\pi I}{F \cos \theta_0} = A_0(\tau, \theta_0, \theta, \phi) + \frac{R f_1(\tau, \theta_0) f_2(\tau, \theta)}{1 - R f_3(\tau)} \quad (1)$$

where I is the backscattered radiance and F the solar flux; θ and θ_0 are the satellite and solar zenith angles, respectively (measured at the ground in the center of instrument field of view); and ϕ is the azimuth angle between the satellite plane and the plane containing the sun. The first term on the right-hand side of (1) is the directional albedo of the earth's atmosphere, f_1 is the fraction of incoming solar radiation reaching the surface, f_2 is the fraction of the reflected radiation emanating in the direction of the satellite, and f_3 is the fraction of the reflected radiation scattered by the atmosphere back to the surface.

The reflectivity R can be calculated by inverting (1), which gives

$$R = \frac{A - A_0(\tau, \theta_0, \theta, \phi)}{f_1(\tau, \theta_0) f_2(\tau, \theta) + [A - A_0(\tau, \theta_0, \theta, \phi)] f_3(\tau)} \quad (2)$$

The atmospheric albedo A_0 and the three fractions, f_1, f_2, and f_3, have been calculated for an atmosphere containing Rayleigh scatterers, using the auxiliary equation solution of the radiative transfer equation developed by *Dave* [1964]. In this procedure the solution is obtained iteratively; each iteration accounts for one additional order of scattering. In practice, the iteration is terminated after the fourth or the fifth order, when the higher-order terms start to follow a simple geometric series, allowing one to extend the series to infinity without additional computation.

The relative contribution of the two terms on the right-hand side of (1), the directional albedo of the earth's atmosphere

[1] Science Applications Research, Lanham, Maryland.
[2] ST Systems Corporation, Hyattsville, Maryland.
[3] Applications Directorate, NASA Goddard Space Flight Center, Greenbelt, Maryland.
[4] National Environmental Satellite Data Information Service, National Oceanic and Atmospheric Administration, Washington, D. C.

Copyright 1987 by the American Geophysical Union.

Paper number 6D0629.
0148-0227/87/006D-0629$05.00

and the surface/atmosphere contribution, is very dependent on the solar zenith angle and the satellite zenith angle. For example, in the case of a surface with a reflectivity of 8% at 380 nm (typical ocean surface reflectivity), a solar zenith angle of 30°, and satellite viewing in the nadir direction, the surface/atmosphere contribution is 23% of the total radiance sensed by the satellite. For the same surface but for a view zenith angle of 60° and a solar zenith angle of 60°, the surface/atmosphere contribution is 12% of the total radiance. Further information on the directional albedo of the earth's atmosphere is given in a tabulation of the Rayleigh atmosphere scattering at 360 nm by *Dave and Furakawa* [1966].

To simplify the operational processing, tables have been calculated for four atmospheric (Rayleigh) optical depths (0.102, 0.180, 0.450, 0.564), corresponding to 0.4 and 1.0 atmosphere pressure at the two TOMS reflectivity channels centered at 360 and 380 nm, at 10 solar zenith angles extending from 0° to 86°, and at six satellite zenith angles extending from 0° to 63°. Function values at the measurement conditions are obtained by interpolation. Surface pressure is estimated using a table of terrain heights. Both of the TOMS reflectivity channels centered at 360 and 380 nm were used to estimate the reflectivity independently, and the average of these two reflectivities, which we will call the TOMS reflectivity at 370 nm, was used in this study.

Precision and accuracy in the computation of R is determined primarily by the precision and accuracy in the measurement of albedo and the accuracy of the terrain height tables. By comparison, the computational error in evaluating the four functions appearing in (2) for specified measurement conditions is negligible ($\sim 0.1\%$).

Since the TOMS instrument measures both the incoming solar flux as well as the earth's backscattered radiance, absolute accuracy in the measurement of the albedo is very high. Most of the instrument's components: the cross-track scanning mirror, the dispersion optics, the analog photodetector, and the instrument electronics, are common to both the solar flux and the earth radiance measurements, so that their individual calibrations do not appear in the computation of albedo. The accuracy in the albedo calibration is determined exclusively by the accuracy with which the reflectivity of an internal diffuser plate (shared by TOMS and the solar backscattered ultraviolet (SBUV) instrument on Nimbus 7 for measuring the solar flux) was known at the time of launch of the satellite and the accuracy with which its subsequent degradation in space has been monitored.

Prelaunch albedo calibration accuracy ultimately depends on the calibration accuracy of the albedo standard maintained by the U.S. National Bureau of Standards (NBS). Accounting for the various steps involved in transferring the NBS calibration to the SBUV/TOMS diffuser, R. P. Cebula, H. Park, and D. F. Heath (Characterization of the Nimbus 7 SBUV radiometer for the long-term monitoring of stratospheric ozone, submitted to the *Journal of Atmospheric and Oceanic Technology*, 1987) estimate that at launch the diffuser reflectivity was known to within $\pm 3\%$ and that it has been monitored to a precision of $\pm 0.5\%$ at the TOMS wavelengths over the life of the instrument. The accumulated error in the TOMS albedo calibration after 6 years of operation is believed to be within $\pm 3.5\%$. This converts to an error of $\pm 2\%$ in surface reflectivity. The TOMS measurement precision is determined by the 1 in 128 precision in converting the analog radiance signal to a digital signal. This translates into a root-mean-square (rms) reflectivity error of 0.3%.

Error in estimating the surface reflectivity can also result from an error in estimating the surface pressure in the instantaneous field of view (IFOV) of the TOMS instrument. Since the terrain height tables used in computing the atmospheric optical depth are given on 2.5° latitude × 2.5° longitude grids, the IFOV atmospheric optical depth is sometimes overestimated in mountainous areas, resulting in an underestimation of the surface reflectivity by up to 3%.

Finally, we consider the errors that may result when the value of R derived from (2) is used to estimate the "scene reflectivity" in the TOMS IFOV. After *Dave* [1976], the quantity "R" obtained from (2) is more properly called the "lambert equivalent reflectivity," which is closely related, though not exactly equal to the bidirectional reflectivity of the scene in the TOMS IFOV. This is because the strong atmospheric scattering at the TOMS wavelengths diffuses both the incoming solar radiation as well as the outgoing reflected radiation, thereby mixing radiation scattered at different angles. *Fraser and Ahmad* [1979] have computed the albedo that is derived from the TOMS reflectivity algorithm at 380 nm for an ocean surface, which is a highly nonlambertian surface. They found that the albedo is strongly overestimated when the wind speed is low (2 m s^{-1}) and both the satellite zenith angle and solar zenith angle are 0°. However, as the difference between solar zenith angle and satellite zenith angle increases to 28°, the albedo derived from the TOMS reflectivity algorithm rapidly approaches the modeled "true" value. Also, for an increased wind speed of 10 m s^{-1} Fraser and Ahmad found a much lower estimate of albedo in the solar glint region of 13%, versus 23% for the 2 m s^{-1} case. For both cases the modeled surface albedo was 4%. It is noted that over most of the ocean surface the wind speed will exceed 2 m s^{-1} and therefore the maximum specular reflection effect will not occur very often. The anisotropy over land surfaces at 370 nm is generally much less than that of ocean surfaces. It is also important to note that the TOMS instrument scans in a direction which is nearly perpendicular to the principal plane of the sun and that this scanning direction minimizes the effects of surface anisotropy, since neither the direct forward-scattering nor the backscattering directions are viewed very often. For a mid level cloud surface, *Taylor and Stowe* [1984] computed the anisotropic factors from the NIMBUS 7 Earth Radiation Budget (ERB) instrument measurements of 0.2- to 4.5-μm radiance as a function of satellite zenith angle and relative azimuth angle to the sun for two extreme solar zenith angle ranges. They found that the anisotropy of the cloud in the plane perpendicular to the principal plane is much less than the anisotropy in the principal plane. However, since the broadband wavelength range of ERB is so dissimilar to TOMS, the magnitude of this anisotropy cannot be used to estimate cloud anisotropy at 370 nm. Nevertheless, it is emphasized that in this paper the word "reflectivity" refers to "lambert equivalent reflectivity," derived using (2), and may differ from the reflectivity of the underlying surface as measured by a surface-based instrument.

3. EARTH SURFACE REFLECTIVITY

To determine quantitatively the surface reflectivity of the earth from TOMS data, we examined the minimum reflectivities measured in a TOMS field of view on a 1° latitude × 1° longitude grid over the whole globe. In the 3-month time period from June through August 1979, TOMS took more than 500 measurements in each of these areas and the absolute minimum of all measurements was selected. This

selection of the minimum value over the 3-month period minimizes the contribution of atmospheric aerosols and solar glint, which tend to increase the inferred reflectivities. Over most of the globe the minimum reflectivities are respresentative of the cloudless reflectivity of the earth's surface, as indicated by the consistency of the reflectivity values between similar surface types scattered widely over the globe (Plate 1). A notable exception is the Intertropical Convergence Zone (ITCZ), where in summer several areas produced no cloud-free observations. There are, in fact, considerable areas of ocean, especially in the tropics and high southern latitudes, where there is some contamination from fractional cloud cover within the TOMS field of view. These ocean areas have a minimum reflectivity of 10–11%, while the more cloud-free ocean areas near subtropical high-pressure systems and near continental boundaries have minimum reflectivity in the range 6–7%. From aircraft flights over the ocean, *Doda and Green* [1980] inferred open ocean reflectivity at 360 and 380 nm to be 6.9% and 7.2%, respectively, for one case (solar zenith of 50.3°–52.5°) and 9.2% and 8.2% for another case (solar zenith of 23.8°–27.2°) under cloudless conditions with some haze present. A few coastal regions have a TOMS reflectivity of 4–5%, and a very few small isolated regions have a reflectivity as low as 2–3%. These are areas of high biomass and chlorophyll density and where there may also be a large amount of dissolved and suspended nutrients and minerals. For example, the coastal areas off of New England and Nova Scotia, which include the rich fishing grounds of the Georges Banks, have a 5% minimum reflectivity. Another interesting example of low ocean reflectivity (3–5%) occurs in the western tropical Atlantic adjacent to the outflow region of the Amazon River. This outflow results in the surface ocean water being largely fresh (nonsaline) for a distance of approximately 160 km from the coast, and this water has a high sediment and nutrient content. Another region of low ocean reflectivity (3–5%) is the open ocean adjacent to the Antarctic ice shelf, which has immense quantities of phytoplankton and zooplankton.

Minimum TOMS reflectivities for large areas of scrub desert in Australia are 2–4%. *Ashburn and Weldon* [1956] also measured the spectral diffuse reflectance of desert surfaces and found the reflectance at 400 nm for brush and windblown sand to be 11.5%. However, Ashburn and Weldon made their measurements in the Mojave desert, where the soil is sandy and alkaline, thus the soil surface may be whiter and brighter than that of brown desert scrub areas. UV reflectance of sandy desert regions, such as the Sahara and Saudi Arabia, are measured by TOMS to typically range from 7–10%. There are some areas within these regions, however, where the TOMS reflectivity is higher (from 11–14%).

Farmland and grassland regions have UV reflectivity similar to scrub desert type areas. TOMS reflectivity over the prairie/farmland area of Kansas/Nebraska is 3–4%, which compares with *Doda and Green*'s [1980] reflectivity values of 3.7% and 4.5% over green farmland and 3.0% and 2.9% over brown farmland at 360 and 380 nm, respectively. Doda and Green's values for farmland, however, are from measurements made from an altitude of 850 feet for green farmland and from 1000 feet for brown farmland and thus are slightly higher than ground-level reflectance because of atmospheric scattering effects. Also consistent with this range of reflectivity for a mixture of tilled land and crops is *Coulson and Reynolds*' [1971] measurements of dry Yolo loam (5–6%) and alfalfa (2–3%) for narrow-band reflectance at 320 and 365 nm.

The reflectance of a pine forest in northern Florida at 360 and 380 nm was found to be 2.3% and 2.6%, respectively, by *Doda and Green* [1980]. In comparison, the spruce-fir forests of central Quebec have a TOMS measured reflectivity of 2% during the summer months. The global map of TOMS minimum reflectivities (Plate 1) also shows reflectivities in the range of 2–3% for the vast coniferous forests of Eurasia.

TABLE 1. Minimum TOMS Reflectivities

Areas	June 1979	September 1979	November 1978
Saharan desert	0.07	0.07	0.06
Kansas/Nebraska	0.03	0.04	0.03
Tropical Atlantic	0.08	0.08	0.06
Saudi Arabia	0.09	0.08	0.07
Quebec (forest)	0.02	0.02	0.12 (snow)

Reflectivities were measured for a 1-week period per month.

There is one type of natural surface for which TOMS measured much higher reflectivity than all other surfaces at 370 nm. This is a salt flat or pan and the only one which is large enough to be resolved by the TOMS field of view is the Salar de Uyuni located in southwestern Bolivia. This region is composed predominantly of sodium chloride with some potassium salts and is roughly 100 × 100 km in size. Therefore near-nadir measurements by TOMS which are centered on this feature are not affected by adjacent surface types. TOMS reflectivities for this salt pan for cloudless conditions during July 1979 range from 57–65%. This variability could be due to nonhomogeneity of the pan or possibly by a small amount of land surface from outside the pan contaminating the field of view. *Hulburt* [1928] measured, under laboratory conditions, a reflectance of 38% for sodium chloride in the spectral band 300–400 nm. *Ashburn and Weldon* [1956] found a reflectivity of 46% at 400 nm for a salt bed in California. The variability could partly be due to differences in spectral bands and also possibly to a variation in salt crystal size and composition.

Table 1 shows values of the minimum TOMS reflectivities for a 1-week period for each of 3 different months for several types of surfaces. Each area identified in Table 1 is a region of 500 × 500 km size. The reflectivities for these examples vary very little from month to month, except for the coniferous forest in Quebec, which had some snow on the ground in November 1978.

Plate 1 shows some mountainous areas having reflectivities of 0–1%. Such low reflectivities may be partially due to the coarse resolution at terrain height correction tables used in the TOMS reflectivity algorithm (section 2).

4. UV Reflectivity of Clouds

The reflectivity of clouds in the UV at 370 nm is qualitatively similar to the visible reflectivity of clouds. A comparison of a map of TOMS reflectivity with a visible Geostationary Operational Environmental Satellite (GOES) image shows a close correspondence between both cloud amount and relative cloud brightness for the two wavelengths. As in visible wavelength images, clouds are bright and ocean and land surfaces are dark. Figure 1*a* is the GOES west visible image for December 3, 1979, at 2045 UT, while Figure 2*b* is the GOES east visible image for the same day at 1700 UT. Both of these GOES satellite images are approximately simultaneous in time with the Nimbus 7 satellite overpass time for the GOES satellite subpoint. Comparing this image with Figure 2, which is a global map of the TOMS UV reflectivity, shows a close correlation of cloud areas between the two images. For exam-

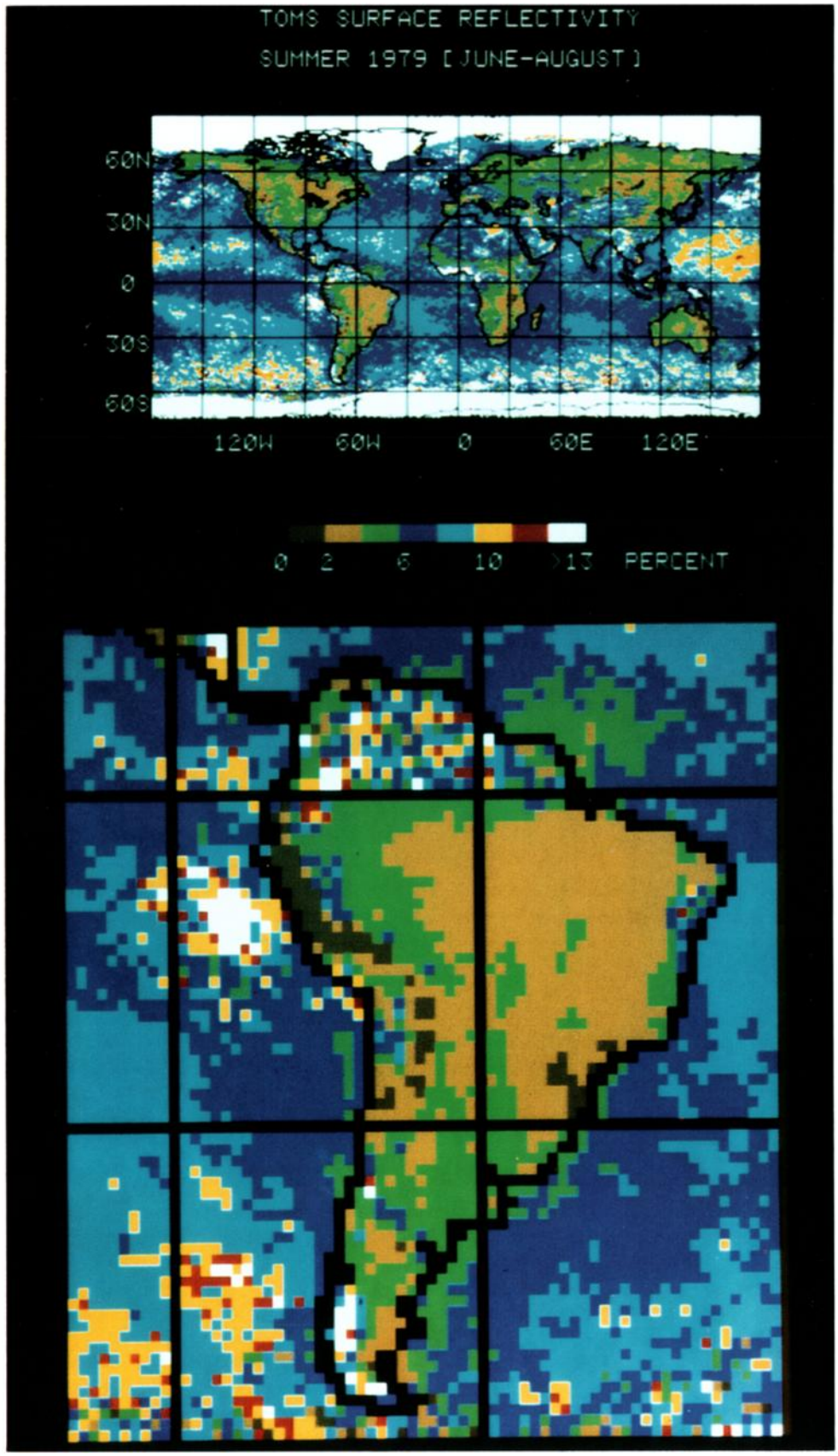

Plate 1. The minimum ultraviolet reflectivity measured by TOMS during the summer of 1979. Each color band in the scale represents a reflectivity interval of 2%. For example, the dark brown is 0–1% reflectivity and the dark blue is 6–7% reflectivity. The similarity between ocean reflectivity and that of the Saharan desert is noted in the top panel. The bottom panel enlargement shows the low ocean reflectivity in the Amazon River outflow region, the cloud-contaminated observations over northern South America, and the persistent stratocumulus off the coast of Peru.

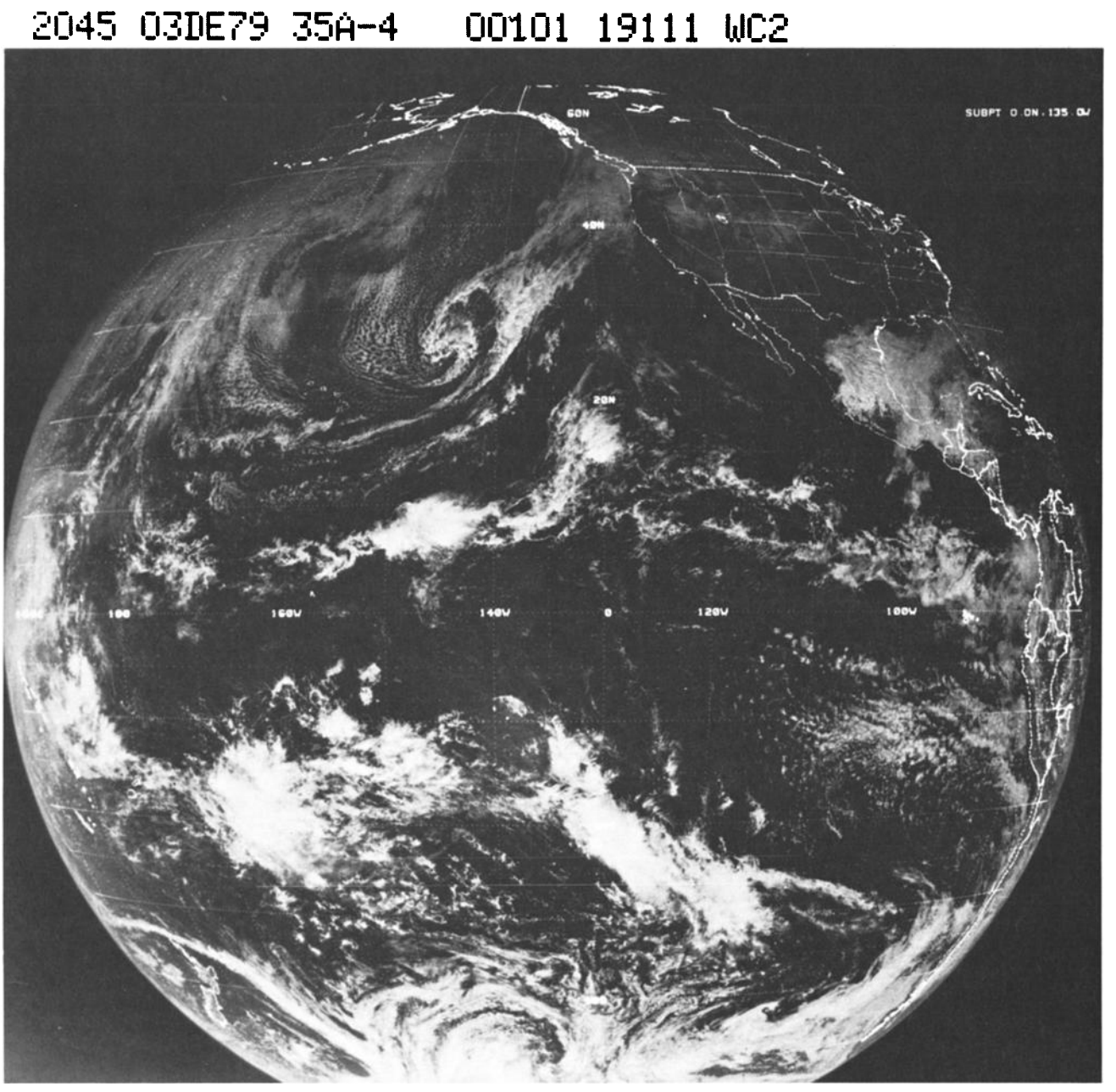

Fig. 1*a*

Fig. 1. The GOES west and GOES east visible images for December 3, 1979, at approximately the same time as the Nimbus 7 overpass. (*a*) GOES west (2045 UT); (*b*) GOES east (1700 UT).

ple, the cyclonic cloud signature west of Baja California in the Pacific Ocean is prominent in both images, as are the two large and very bright cloud masses in the south central Pacific. It is also noted that the stratocumulus and the broken to scattered cumulus cloud field off the coast of Peru is also measured by the TOMS instrument to be a lower reflectivity cloud field. Although these comparisons demonstrate the qualitative similarities in cloud reflectance between visible and UV images, a quantitative comparison is limited by the lack of visible reflectance data. However, the theoretical study of *Novoseltsev* [1964] found that for a "middle layer" water droplet cloud of 500 m thickness the reflectivity remains practically constant from 200 to approximately 700 nm.

The average cloud reflectivity on a global scale was determined for clouds at three different cloud-top altitudes by using an independent determination of cloud fraction and altitude. It is noted that the "cloud" reflectivity is more accurately described as the "overcast atmosphere/surface" reflectivity, since some of the atmosphere/surface underlying the cloud might be sensed by the TOMS radiometer, depending on the cloud optical depth at 370 nm. For simplicity, however, we will refer to these reflectivities as cloud reflectivity. The cloud climatology data set described by L. L. Stowe, C. G. Wellemeyer, T.F. Eck, H. Y. M. Yeh, and the Nimbus 7 Cloud Data Processing Team (Nimbus 7 global cloud climatology, I, First year results, submitted to the *Journal of Climate and Applied Meteorology*, 1986) was used to identify completely cloud-covered fields of view. Briefly, this algorithm uses the Temperature Humidity Infrared Radiometer (THIR) infrared (11.5 μm) radiometer which is also on board Nimbus 7, in conjunc-

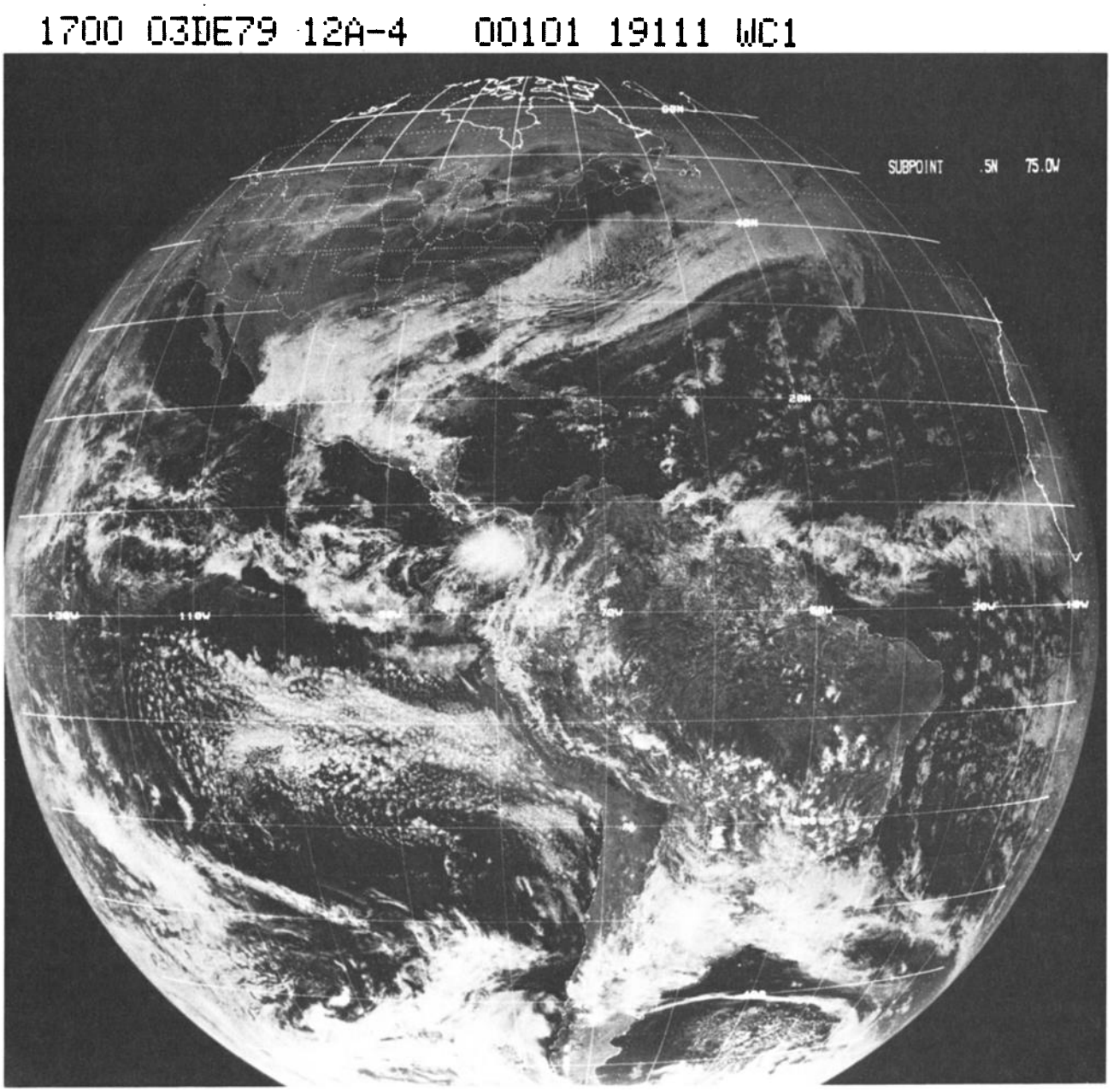

Fig. 1*b*

Fig. 1. (continued)

tion with the Air Force three-dimensional nephanalysis surface temperature data set, to determine cloud amount. The THIR instrument FOV is 6.7 km at nadir and about 50–100 THIR field of views are colocated into one TOMS field of view. Cloud-top altitude is determined for three categories from a geographical and seasonal climatology of temperature lapse rates which were compiled at the National Center for Atmospheric Research (NCAR) in Boulder, Colorado by *Jenne et al.* [1974]. The three cloud top height categories are (1) low cloud, 0–2 km; (2) midcloud, 2–7 km at the equator, varying with latitude to 2–4 km at the poles; and (3) high cloud, greater than 7 km at the equator to greater than 4 km at the pole. The decrease in cloud-top altitude from equator to pole is designed to follow changes in tropopause height with latitude. Table 2 shows the global average mean and standard deviation of the TOMS reflectivity for each of the three cloud-top height categories. These data represent average reflectivities of clouds between 60°N and 60° S and have been obtained from cases where the infrared cloud algorithm identified 100% cloud for the TOMS field of view. Even though the anisotropic reflection characteristics of clouds have not been accounted for, both as a function of solar zenith angle and satellite zenith angle, it is felt that these effects are not dominant when compared to the great variability in cloud types and their optical properties. Again, it is noted that the TOMS instrument scans in a direction which is close to perpendicular to the principal plane of the sun and this scan direction minimizes anisotropic view angle effects (see section 2). UV cloud

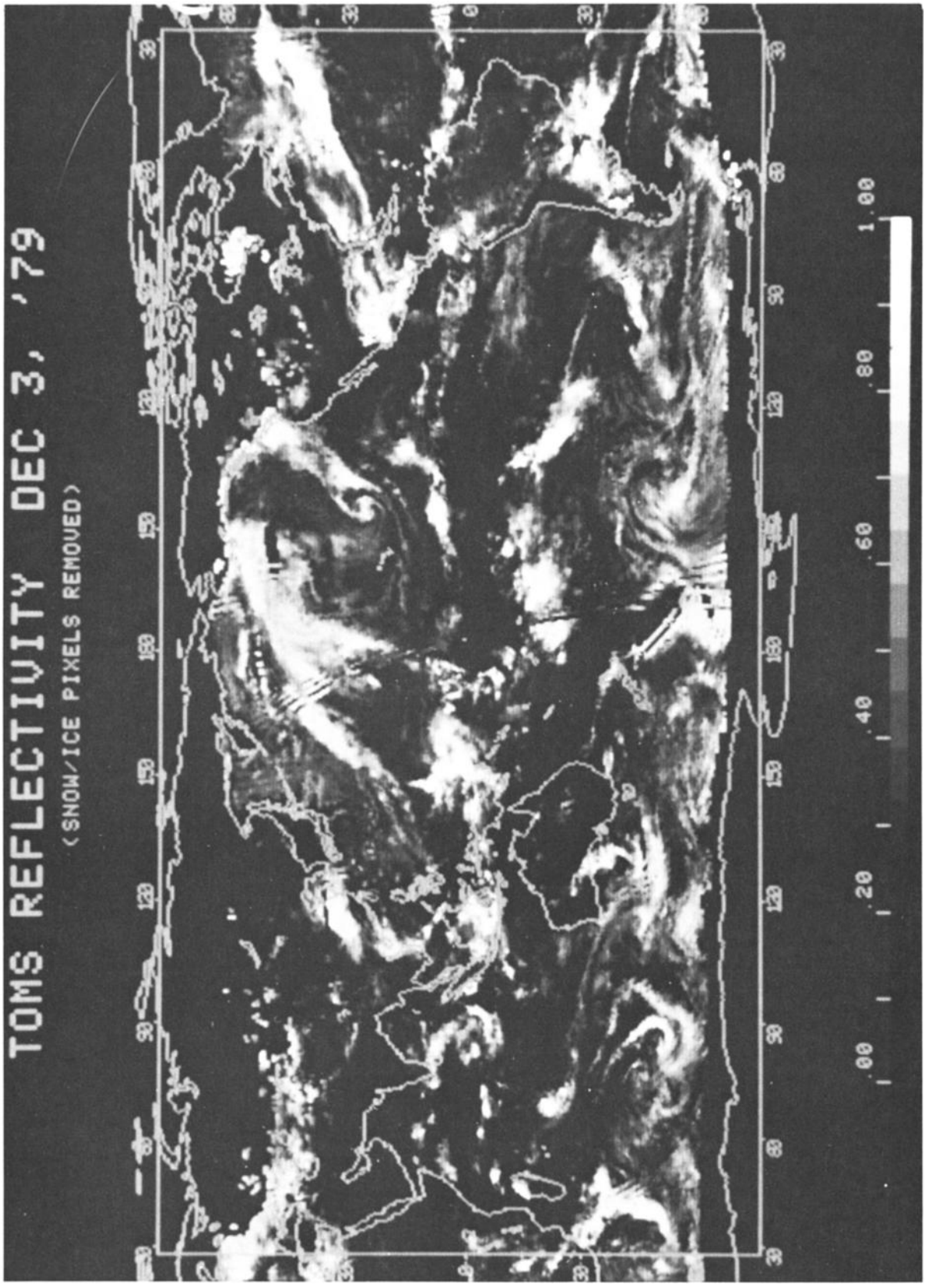

Fig. 2. The ultraviolet reflectivity measured by TOMS on the same day as the GOES images in Figure 1. There is a close correspondence between the cloud features in the visible GOES images with those in the UV TOMS map.

TABLE 2. TOMS Reflectivities for 100% Cloud-Filled FOVs for the Time Period June 24–30, 1979, From 60°N to 60°S

	Mean	Standard Deviation	Number of Observations
Low cloud only	51.5	16.2	1,512
Mid cloud only	57.0	16.2	30,648
High cloud only	76.0	13.5	25,127
Total cloud	56.1	20.3	177,934

reflectivity shows a significant increase with increasing cloud-top height. *Park et al.* [1974] found high negative correlations between cloud-top temperatures, measured by Nimbus 4 THIR, and visible brightness, measured from the ATS 3 satellite, for cloud fields containing cumulonimbus clouds. *Kaveney et al.* [1977] found a correlation between cloud thickness derived from pilot reports and reflected visible radiation measured from the NOAA 4 satellite. This observation is supported in theory by *Twomey et al.* [1967], who showed an exponential increase in cloud albedo with increasing cloud thickness. Maximum cloud thickness of clouds in our low-cloud category is 2 km, while the maximum thickness for high clouds can be as large as 10 km in the tropics for cumulonimbus clouds. Since cloud-top height determines the three cloud categories, there is a variety of cloud thickness and density types being averaged into each cloud category. For example, the infrared determination of cloud top level for thin cirrus cloud is usually midcloud, since there is a transmission of radiation from warmer underlying surfaces through a thin high cirrus cloud. *Frederick and Abrams* [1981] found a typical average cloud albedo to lie in the range 50–60% from the AE-E satellite measurements taken at 330–340 nm. This range is in good agreement with the mid-cloud and low-cloud TOMS reflectivities.

Since the size of the TOMS field of view (FOV) varies from 50 × 50 km to 150 × 200 km, a large percentage of the FOVs contain partial cloud cover. Figure 3 shows the average values of the THIR infrared cloud algorithm percent total cloud cover versus TOMS reflectivity. The average percent reflectivity at each point is representative of a 5% cloud amount interval. Thus for example, for the cloudiness range of 50–55% the average TOMS reflectivity is 29%. This is an average reflectivity of course and there is a wide variation in reflectivity for different cloud thicknesses and types. A 100% cloud-filled FOV for a cumulonimbus cloud may have a typical TOMS reflectivity of 70–80%, while a 100% cloud-filled FOV of thin cirrus cloud may have a typical reflectivity of 15–25%.

In Figure 3 it is noted that there is an apparent discrepancy between the UV reflectivity and cloud amount for small cloud amounts, especially for the range 0–20% cloudiness. For example, the average reflectivity for the 5–10% cloud interval is 18.1%, which would indicate that the cloud reflectivity is greater than 100%, given that the typical background surface (ocean) reflectivity is 7–8% (see previous section). The reason for this relatively high scene reflectivity at small infrared (IR) detected cloud amounts is due to the inability of the IR cloud algorithm to detect clouds which have very little thermal contrast with the underlying surface. Therefore there are a significant number of cases which, in reality, have more cloud than is detected by the IR algorithm. These cases are averaged in with observations of higher altitude (greater thermal contrast) cloud in the computation of the mean reflectivity for each cloud percentage interval.

Figure 4 is a global map of the TOMS reflectivity averaged for the month of July 1979. The reflectivity values which are mapped are averages over a grid with element size of 480 × 480 km, and the wavy line at 65°–70°S is the polar night delineator, thus there is no reflectivity data below this line. For comparison, Figure 5 shows the THIR total cloud climatology from the IR algorithm for the same month. In comparing these two maps it is noted that the arid land regions of the world and also the oceanic subtropical high-pressure areas have both low UV reflectivity and low total cloud amount. Also the ITCZ and the southeast Asian mon-

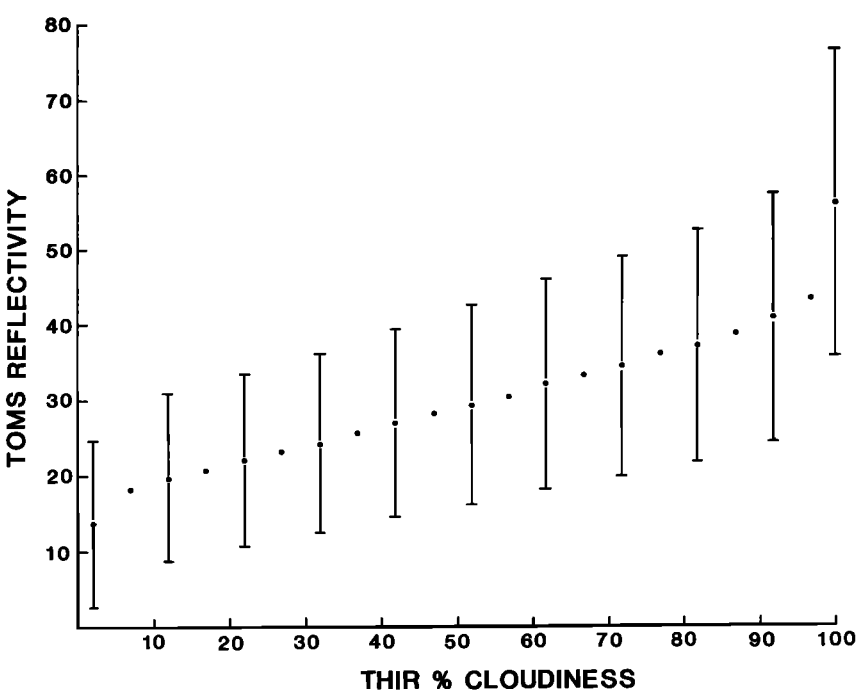

Fig. 3. TOMS reflectivity as a function of THIR total cloud amount, from 60°S to 60°N, for the week June 24–30, 1979. The bars denote plus and minus one standard deviation.

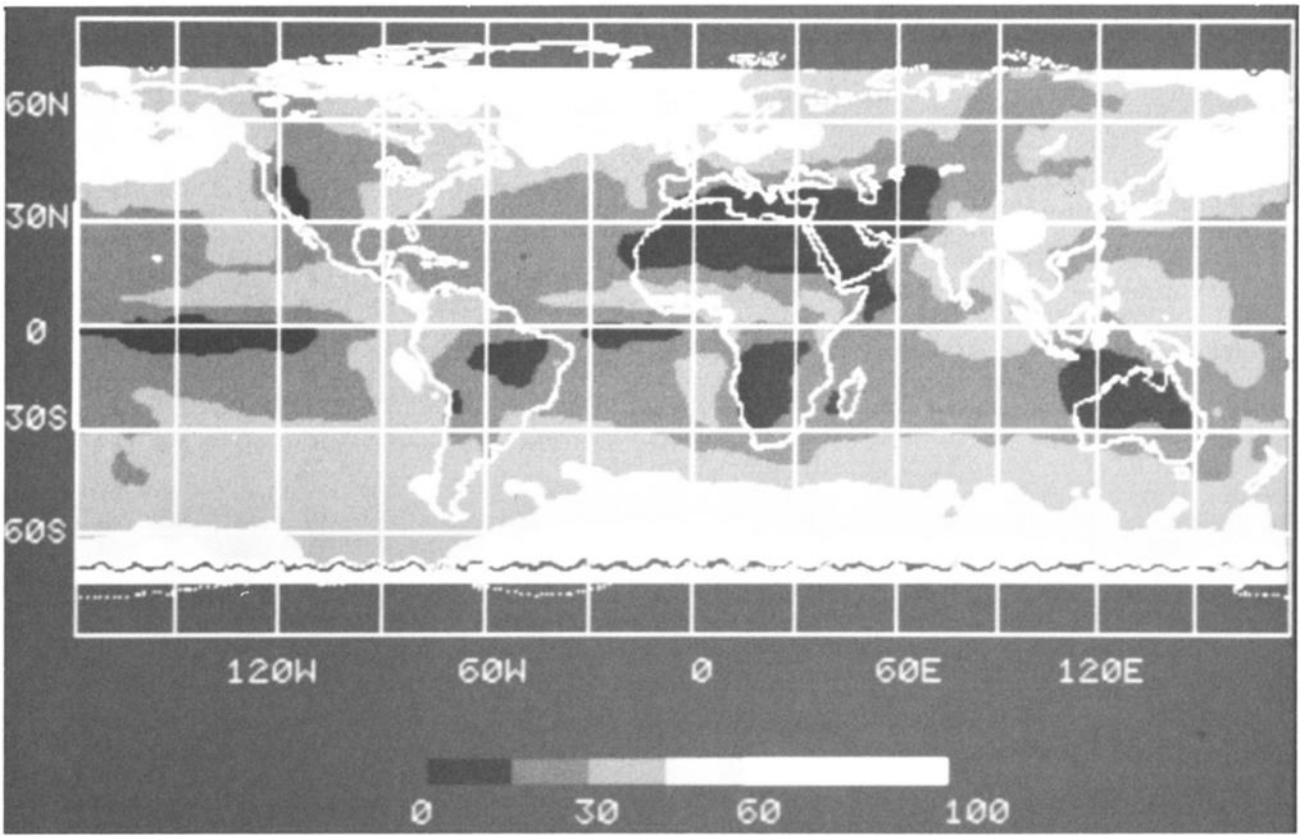

Fig. 4. Average monthly UV reflectivity measured by TOMS for July 1979. Note the low reflectivity over arid land regions and the high reflectivity over the Greenland ice cap.

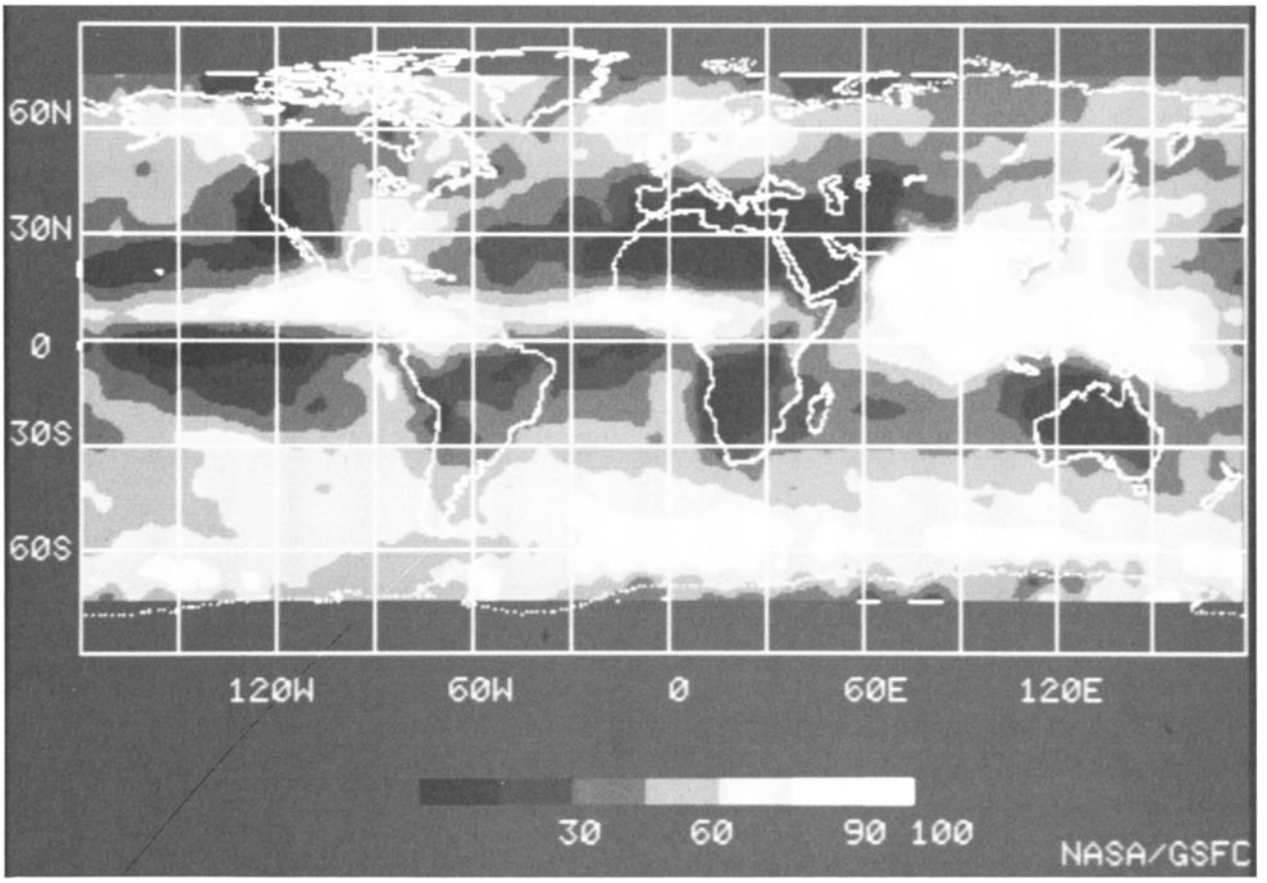

Fig. 5. Average monthly total cloud cover for July 1979, determined from the infrared channel on THIR. The THIR and TOMS measurements are taken simultaneously at near local noon. There is a correspondence between the total cloud cover and the TOMS reflectivity in Figure 4.

soon region are prominent features both in the total cloud amount and the average reflectivity. The region of highest UV reflectivity in Figure 5 is the Greenland ice cap and a few Arctic Ocean areas which are frozen and also some of the ocean areas adjacent to Antarctica.

Comparison of the UV reflectivity map and the IR-derived cloud map (Figures 4 and 5) also reveals some apparent inconsistencies in the relation between cloud amount and cloud reflectivity. For example, the region north of central Australia at about 5°N latitude has 90–100% cloud detected in the IR and the UV reflectivity is 30–45%, while in the region off the coast of Peru the IR cloud amount is less at 60–75% but the UV reflectivity is greater at 45–60%. This is due to the variability in cloud thickness for different regions of the world, with there being relatively high reflectivity for the homogeneous stratocumulus cloud layer off the Peru coast, while the average reflectivity in the Indonesian area is reduced by the presence of large amounts of thin cirrus and low-altitude clouds.

5. Conclusions

UV reflectivities at 370 nm measured by the TOMS instrument on Nimbus 7 are able to resolve all the significant cloud features, which is apparent in comparison to a GOES visible image. Using THIR infrared radiances to determine cloud amount and height, the TOMS reflectivities for low clouds (below 2 km) average 51.5%, for midlevel clouds (from 2 km to 4–7 km) average 57.0%, and for high clouds (above 4–7 km, depending on latitude) average 76.0%. This increase in UV reflectivity with cloud-top altitude is apparently due to an increase in the average cloud thickness.

UV reflectivities for cloudless scenes measured by TOMS typically vary from 2–9% for most types of land and water (ocean) surfaces. These reflectivities are in excellent agreement with measurements made of similar surface types from aircraft at 360 nm and 380 nm. The typically low surface reflectivities in UV allow for the detection of clouds over deserts and coastal areas where visible and infrared techniques may have problems.

A few earth surface types have UV reflectivities of greater than 9%. These areas include some areas of the Saharan desert (Libyan desert especially) and some parts of Saudi Arabia with reflectivity ranging from 10–14%. These areas are a relatively small percentage of the total desert areas, however. One other notable exception is the Salar de Uyuni, a large salt flat in southwestern Bolivia, which has a UV reflectivity of ~60%.

Acknowledgments. The authors would like to thank E. Hurley and A. Fleig of NASA Goddard Space Flight Center for their support and encouragement of our work on the Nimbus 7 THIR/TOMS cloud data set. We also thank the anonymous reviewers for their useful comments, which have resulted in improvement of the presentation of these results.

References

Ashburn, E. V., and R. G. Weldon, Spectral diffuse reflectance of desert surfaces, *J. Opt. Soc. Am.*, *46*, 583–586, 1956.

Coulson, K. L., and D. W. Reynolds, The spectral reflectance of natural surfaces, *J. Appl. Meteorol.*, *10*, 1285–1295, 1971.

Dave, J. V., Meaning of successive iteration of the auxillary equation in the theory of radiative transfer, *Astrophys. J.*, *140*, 1292–1303, 1964.

Dave, J. V., Investigation of the effect of atmospheric dust on the determination of total ozone from the earth's ultraviolet reflectivity measurements, *Access. N77-24690, 24691, 24692*, Natl. Tech. Inf. Serv., Springfield, Va., 1976.

Dave, J. V., and P. M. Furakawa, Scattered radiation in the ozone absorption bands at selected levels of a terrestrial, Rayleigh atmosphere, *Meteorol. Monogr.*, *7*(29), 353 pp., 1966.

Doda, D. D., and A. E. S. Green, Surface reflectance measurements in the UV from an airborne platform, 1, *Appl. Opt.*, *19*, 2140–2145, 1980.

Fraser, R. S., and Z. Ahmad, The effect of surface reflection and clouds on the estimation of total ozone from satellite measurements, Fourth NASA Weather and Climate Program Science Review, edited by E. R. Kriens, *NASA Conf. Publ. CP-2076*, 1979.

Frederick, J. E., and R. B. Abrams, The surface albedo of the earth in the near ultraviolet (330–340 nm), *Remote Sens. Environ.*, *11*, 337–347, 1981.

Hulburt, E. O., The ultraviolet, visible, and infrared reflectivities of snow, sand, and other substances, *J. Opt. Soc. Am.*, *17*, 23–25, 1928.

Jenne, R. L., H. L. Cruthcer, H. Van Loon, and J. J. Taljaard, A selected climatology of the southern hemisphere: Computer methods and data availability, *Tech. Note NCAR-TN/STR-92*, Natl. Cent. for Atmos. Res., Boulder, Colo., 1974.

Kaveney, W. J., R. G. Feddes, and K. N. Liou, Statistical inference of cloud thickness from NOAA 4 scanning radiometer data, *Mon. Weather Rev.*, *105*, 99–107, 1977.

Novoseltsev, Y. P., Spektrolnaya Otrazhatelnaya Oblakov, *Tr. Gla.: Geofiz. Obs. A. D. Voyykova*, (Spectral Reflectivity of Clouds, Engl. Transl., *NASA TT F-328*(152), pp. 186–197, 1964).

Park, S-U., D. N. Sikdar, and V. E. Suomi, Correlation between cloud thickness and brightness using Nimbus 4 THIR data (11.5-μm channel) and ATS 3 digital data, *J. Appl. Meteorol.*, *19*, 1341–1350, 1974.

Taylor, V. R., and L. L. Stowe, Reflectance characteristics of uniform earth and cloud surfaces derived from Nimbus 7 ERB, *J. Geophys. Res.*, *89*, 4987–4996, 1984.

Twomey, S., H. Jacobowitz, and H. B. Howell, Light scattering by cloud layers, *J. Atmos. Sci.*, *24*, 70–79, 1967.

P. K. Bhartia, ST Systems Corporation, 5809 Annapolis Road, Hyattsville, MD 20784.

T. F. Eck, Science Applications Research, 4400 Forbes Boulevard, Lanham, MD 20706.

P. H. Hwang, Applications Directorate, NASA Goddard Space Flight Center, Greenbelt, MD 20771.

L. L. Stowe, National Environmental Satellite Data Information Service, National Oceanic and Atmospheric Administration, Washington, DC 20233.

(Received January 30, 1986;
revised October 20, 1986;
accepted October 22, 1986.)